

A Novel litchi-like Fe₃O₄/graphene Composite Catalyst for the Lithium–Air Battery

Hui Lv, Rongli Jiang*, Xiaoyu Zhang, Jing Wang, Yanfen Li

College of Chemical Engineering and Technology, China University of Mining and Technology, Xuzhou 221116, China

*E-mail: ronglijcumt@163.com

Received: 18 June 2015 / Accepted: 12 July 2015 / Published: 28 July 2015

A novel litchi-like Fe₃O₄/graphene composite as a cathode material of lithium–air batteries was successfully synthesized by an effective solvothermal method, with cheap and eco-friendly iron salts. The litchi-like Fe₃O₄ nanoparticles (NPs) which could provide a larger electrochemical reaction surface were ~250 nm in size and homogeneously distributed onto the surface of conducting graphene sheets. Owing to synergistic effect between the litchi-like Fe₃O₄ nanoparticles and graphene sheets, Fe₃O₄/graphene composites (Fe₃O₄/GCs) exhibited much higher electrocatalytic activity compared to the Fe₃O₄ NPs. The charge/discharge tests showed that the lithium–air battery based on the litchi-like Fe₃O₄/graphene composite had an excellent discharge capacity of ~1638 mA h g⁻¹ at a voltage of 2.0–4.1 V at 50 mA g⁻¹, and also exhibited low charge potential and improved the energy efficiency as well as reversible capacity.

Keywords: Litchi-like Fe₃O₄ nanostructures; Graphene; Composite; Lithium–air batteries

1. INTRODUCTION

Development of effective electrocatalysts is a key stage for the development of practical rechargeable Li–air batteries. The electrocatalysts not only prevent the side reactions but also promote the slow kinetics related to oxygen reactions [1]. They play a key role in improving the power density, cyclability, and energy efficiency [2]. Electrochemically active transition metal oxides (MnO₂, Co₃O₄, RuO₂, Fe₂O₃, NiO, CuO, Fe₃O₄, and Mn₃O₄) have been widely investigated as oxygen electrocatalysts for Li–air batteries [3–10]. Among the transition metal oxides, magnetite is regarded as promising candidate electrocatalyst for Li–air batteries because of its abundance, low cost, being eco-friendly, having superior electrical conductivity [11].

Ultrathin flexible graphene sheets are excellent nanoscale building blocks for hybrid materials. Unique two-dimensional graphene can effectively enhance the electrochemical performance of these nanomaterials because of its high electrical conductivity, high chemical stability, well-defined porosity, and high surface area [1,12–14]. Graphene and graphene-based composites have been extensively used in Li–air batteries. Graphene has two main advantages as a support for anchoring NPs in Li–air batteries. First, graphene sheets can effectively prevent the aggregation of NPs and produce well-dispersed NPs. Second, they can improve charge transfer during the charge/discharge process due to their intrinsic high electronic conductivity and good contact between the graphene and the Fe₃O₄ NPs.

Fe₃O₄/graphene composites have the advantages of the respective properties of each component to achieve the synergistic effect between the graphene and the Fe₃O₄ NPs [15,16]. Common synthesis methods of Fe₃O₄/graphene composites include the hydrothermal, solvothermal, and co-precipitation methods [17–19]. However, the synthesis of the hybrid of graphene homogeneously modified with Fe₃O₄ NPs with controlled morphology, dispersion, and size, remains a major challenge and is needed in order to expand the potential applications of Fe₃O₄ nanomaterials.

In this study, we synthesized a novel litchi-like Fe₃O₄/graphene composite as a catalyst cathode electrode for Li–air batteries via the solvothermal process. The morphology, particles size, structure, and electrochemical properties of this as-prepared composite were investigated in detail by X-ray diffraction (XRD), Fourier transform infrared spectroscopy (FTIR), field emission scanning electron microscopy (FE-SEM), and transmission electron microscopy (TEM) measurements. Furthermore, the charge/discharge property and impedance of the cells, are investigated and compared in order to understand the performance of lithium–air cells using an air electrode with a Fe₃O₄/graphene composite or Fe₃O₄ NPs catalysts. The electrode reaction products were analyzed.

2. EXPERIMENTAL

Graphite oxide (GO) used in this work was prepared from natural graphite powder by the modified Hummers method as previously reported [20–24]. The Fe₃O₄/graphene composites were synthesized by a solvothermal process. In a typical procedure, 0.16 g of graphite oxide was dispersed in 90 ml of ethylene glycol by ultrasonication for 30 min. Subsequently, 0.8 g of ferric chloride hexahydrate and 0.56 g of hexamethylene-tetramine (HMTA) were added into the GO solution and then stirred at room temperature for 1 h. Then 5.0 g of polyethylene glycol (PEG) and 0.57 g of sodium acetate trihydrate were dropped into the mixture with magnetic stirring for 1 h. The mixture was then transferred to a 150 mL Teflon-lined stainless steel autoclave and sealed. After solvothermal treatment at 200 °C for 22 h, the reaction was finished and cooled to room temperature. The products were separated by a magnet and were washed several times with de-ionized water and ethanol, and then dried by a suitable treatment. Finally, the Fe₃O₄/GO nanocomposites were vacuum-dried at 50 °C for 3 h, and then slowly heat treated to 500 °C under a nitrogen atmosphere in a tubular furnace and maintained at this temperature for 2 h. Then, the sample was cooled to room temperature, naturally and

Fe_3O_4 /graphene composites were obtained. Fig. 1 shows the flowchart of the synthesis process of Fe_3O_4 /graphene nanocomposites.

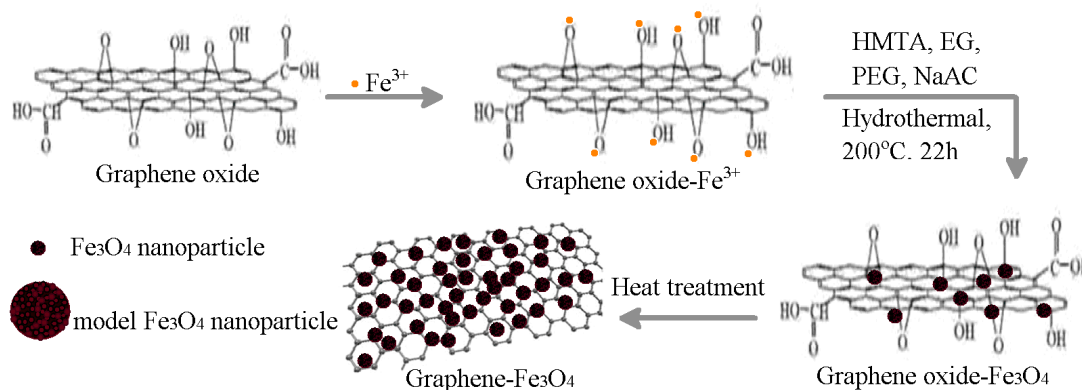


Figure 1. A scheme for the synthesis process and the structure of Fe_3O_4 /graphene nanocomposite.

The structures of the as-prepared materials were analyzed with Cu- $K\alpha$ radiation (at $\lambda=0.15406$ nm, 40 kV, 30 mA) on a Bruker AXS D8 X-ray diffractometer (XRD). Hitachi SU8020 field emission scanning electron microscopy (FE-SEM, Hitachi Limited) and transmission electron microscopy (TEM, JEOL-JEM2100F) with an accelerating voltage of 200 kV were used to observe the morphologies and microstructure of the as-prepared materials. Fourier transform infrared spectroscopy was recorded from 400 to 4000cm^{-1} with a Nicolet NEXUS spectrometer using pressed KBr pellets. The mass percentage of Fe_3O_4 and graphene in the composite were determined by thermogravimetric analysis (HCT-3, Hengjiu scientific instruments company, Beijing, China) in air with a heating rate of $10^\circ\text{C min}^{-1}$ from room temperature to 1000°C .

The air electrodes were prepared by dispersing a mixture of acetylene black, catalyst (the prepared Fe_3O_4 /graphene composites), and a polyvinylidene fluoride (Kynar FLEX 910, Elf Atochem, Issaquah, WA, USA) binder (mass ratios: 5:1:4) dissolved in N-methyl pyrrolidone (Fluka Inc., St. Louis, MO, USA) onto a Cu foil current collector. The electrodes were incorporated into cells with Li foil and 1 M LiPF_6 in ethylene carbonate (EC)/ethylmethyl carbonate (EMC)/dimethyl carbonate (DMC) (weight ratios: 1:1:1, Guotaihuarong company, Zhangjiagang, China) as the electrolyte. Seven holes with a diameter of 2 mm were opened on the shell of the Li-air coin cell (CR2032-type) for the diffusion of oxygen. To prevent the moisture content in the air reacting with the lithium electrode, a waterproof breathable layer (Neware, Shenzhen, China) was used as a protective layer on the surface of the cell. All electrochemical measurements of Li-air coin cells were carried out in the air. The galvanostatically charge/discharge tests were carried out on a battery analyzer (VoiR, Huizhou, China) over a range of 1.5–4.5 V (vs. Li/Li^+) at room temperature. EIS measurements were performed in an electrochemical work station (Solartron 1287, Solartron Co., England). The amplitude of the AC perturbation signal was 5 mV and the frequency range varied from 10^5 to 10^{-2} Hz.

3. RESULTS AND DISCUSSION

The crystalline structure of as-prepared GO and Fe₃O₄/graphene nanocomposites were characterized by X-ray diffraction (XRD) (Fig. 2(a)). As shown in Fig. 2(A), a broad diffraction peak at $2\theta=13.9^\circ$, corresponds to the (0 0 1) reflection of GO. The XRD pattern of the composites is shown in Fig. 2(B), all the diffraction peaks of Fe₃O₄ could be indexed to the inverse cubic spinel structure of Fe₃O₄ (JCPDS No. 65-3107). There was an obscure weak diffraction near 25.88° from the graphene sheets suggesting that the short-range ordering in the crystal structure and the graphene sheets had been uniformly distributed in the composites. These results indicated that Fe₃O₄/graphene nanocomposites were obtained.

The typical TGA curve of the as-prepared Fe₃O₄/graphene nanocomposite is presented in Fig. 2(b). As shown in the curve, the Fe₃O₄/graphene nanocomposite showed a weight loss between room temperature and 130 °C, because of the liberation of adsorbed water. The mass increase between 130 °C and 300 °C can be attributed to the oxidation of Fe₃O₄ to Fe₂O₃. A drastic weight loss between 300 °C and 520 °C was caused by the decomposition of graphene nanosheets [25]. The weight percentages of graphene and Fe₃O₄ in the nanocomposites could be calculated from the weight losses of graphene and the mass gains of the oxidation of Fe₃O₄ to Fe₂O₃, which were about 20 wt.% and 80 wt.%, respectively.

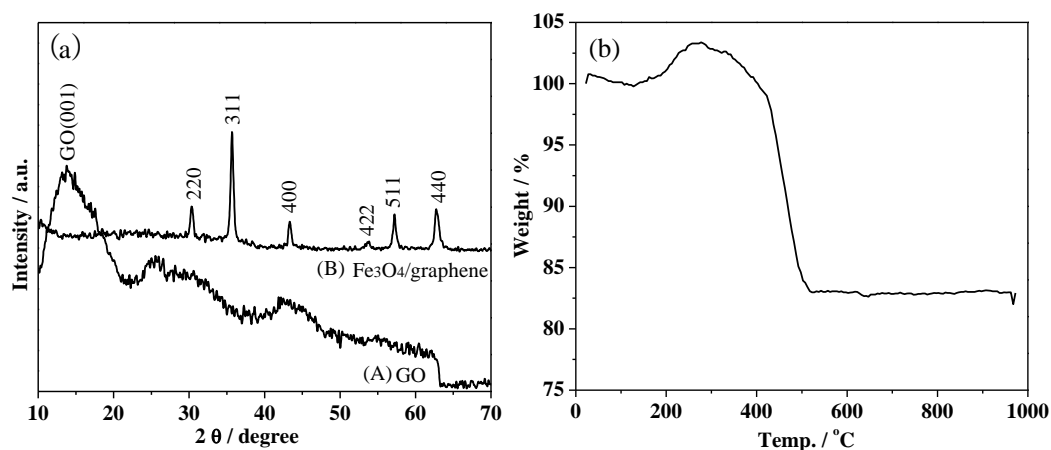


Figure 2. (a) XRD patterns of (A) GO and (B) Fe₃O₄/graphene and (b) TGA curve of Fe₃O₄/graphene nanocomposite.

The integration of GO and Fe₃O₄/graphene composites were further confirmed by structural analysis with FTIR spectroscopy. Fig. 3 shows the FTIR spectra of GO (Fig. 3(A)) and the as-prepared Fe₃O₄/graphene composites (Fig. 3(B)). In both the spectra of GO and Fe₃O₄/graphene, there were some uniform peaks of the groups. The wide peak at 3442 cm^{-1} was associated with stretching of the O–H. The weak peak located at 2360 cm^{-1} was ascribed to the stretching of C–H. Stretching vibration of the C=O bond of carboxy on the surface of GO was observed as the band present at 1635 cm^{-1} . The band at 1340 cm^{-1} was attributed to the bending vibration of the O–H bond of the adsorbed H₂O. The

peak at 1090 cm^{-1} was attributed to the C–O stretching vibration. The band at 578 cm^{-1} , which presented in the FT-IR spectrum of $\text{Fe}_3\text{O}_4/\text{graphene}$, was assigned to Fe–O stretching vibration confirming the existence of Fe_3O_4 . This result revealed there were few oxygen-containing functional groups left in $\text{Fe}_3\text{O}_4/\text{graphene}$.

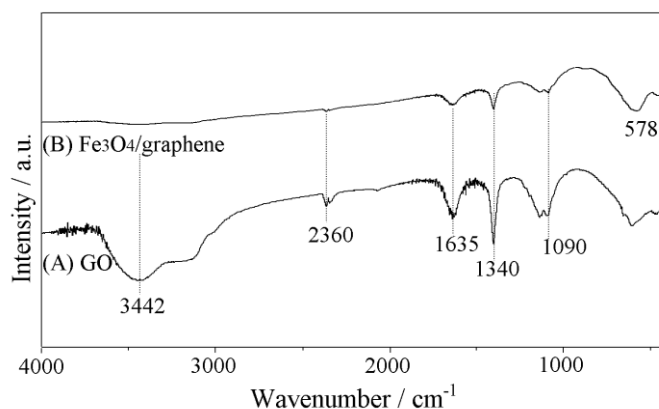


Figure 3. FTIR spectra of (A) GO and (B) $\text{Fe}_3\text{O}_4/\text{graphene}$ nanocomposite.

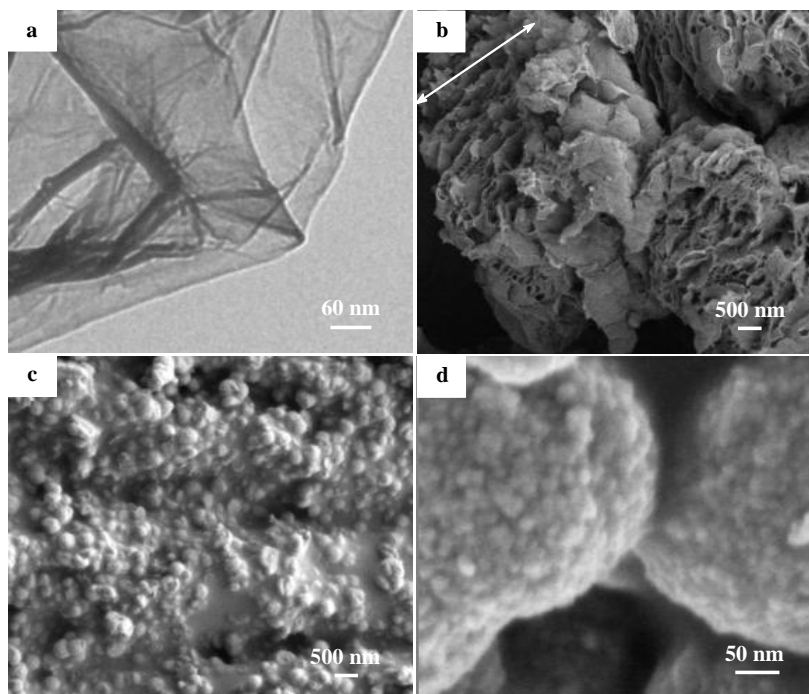


Figure 4. TEM (a) and SEM (b) images of GO, and low-magnification (c) and high-magnification (d) SEM images of $\text{Fe}_3\text{O}_4/\text{graphene}$ nanocomposites.

The morphologies and structure of GO and $\text{Fe}_3\text{O}_4/\text{graphene}$ were examined by TEM and SEM. Fig. 4(a) shows TEM image of GO, which presents a typical wrinkled and stacked morphology. The typical SEM image Fig. 4(b) shows that the individual graphene oxide sheets as the building blocks were stacked layer-by-layer into the GO membrane, and the thickness of the GO membrane was about

4 to 5 μm . From the image it was found that the surface of graphene sheets was decorated with Fe_3O_4 nanoparticles with an average diameter of ~ 250 nm (Fig. 4(c)). Fig. 4(d) shows a high magnification SEM image of the Fe_3O_4 particles which were coated on the surface of graphene. The particles were novel litchi-like in shape and evenly distributed. The surface of Fe_3O_4 s was coarse, but closer inspection revealed an ordered assembly of nanoparticles. This can give rise to a high specific surface area, which will then result in better electrochemical properties.

Fig. 5 shows the initial charge/discharge voltage profiles of the lithium–air battery using the air electrode with the Fe_3O_4 /graphene composite and Fe_3O_4 NPs catalysts at 50 mA g^{-1} in the potential window of 4.1–2.0 V versus Li/Li^+ . The cell based on Fe_3O_4 NPs has an initial discharge capacity of 1000 mA h g^{-1} , if normalized by the total electrode mass (acetylene black + binder + catalyst) (Fig. 5(a)). The cell based on Fe_3O_4 /graphene composite delivers higher discharge capacity of 1638 mA h g^{-1} under the same current density (Fig. 5(b)). The discharge plateau of the lithium–air battery based on Fe_3O_4 /graphene composite was flat at 2.72 V and the charging potential plateau was flat at 3.76 V with high reversible capacity. It was 0.09 V higher and 0.02 V lower than that of the lithium–air battery based on Fe_3O_4 NPs, respectively. The difference between the charge and discharge voltage (ΔV) was ~ 1.04 V, the energy efficiency of $\sim 72\%$ was obtained for Li–air cells using Fe_3O_4 /graphene composite as a catalyst. It was 0.12 V lower and 3% higher than that of the lithium–air battery based on Fe_3O_4 NPs, respectively. This was because the unique litchi-like Fe_3O_4 within the Fe_3O_4 /graphene composite could provide a larger electrochemical reaction surface and the synergistic effect between the Fe_3O_4 NPs and the graphene sheets. The carbon atoms at the edge of graphene nanosheets are considered to be “partially radical”, which can offer special chemical reactivity, and might serve as active sites for the electrochemical reaction of oxygen [26]. It showed that the application of Fe_3O_4 /graphene composite catalyst for Li–air cell is effective for decreasing the charging potential plateau. Therefore, Fe_3O_4 /graphene composite electrode was highly active to a Li–air cell.

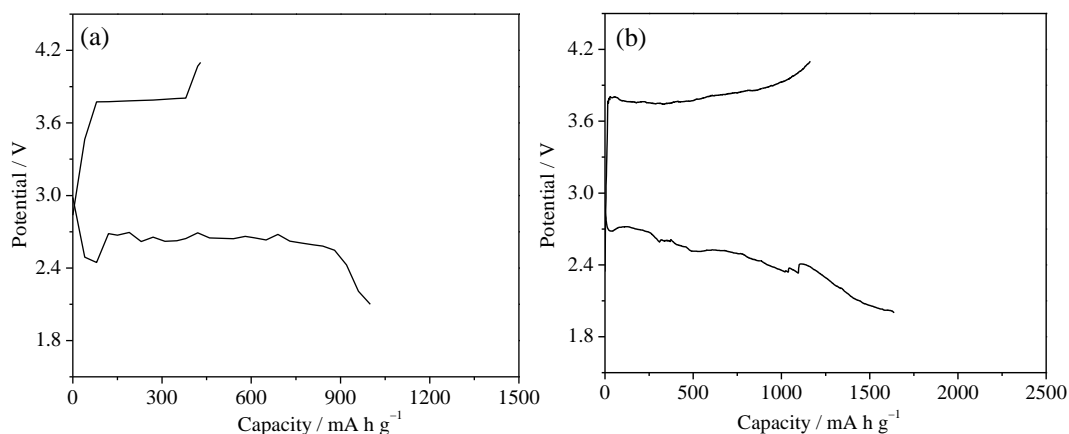


Figure 5. The initial charge/discharge curves of Li–air cell using air electrode with different catalysts at a current density of 50 mA g^{-1} between 2.0 and 4.1 V. (a) Fe_3O_4 NPs; (b) Fe_3O_4 /graphene nanocomposite

The electrochemical impedance spectra (EIS) of the Li–air coin cell using an air electrode with a Fe_3O_4 /graphene composite catalyst were recorded before and after discharge, as shown in Fig. 6(a).

Such a pattern of EIS was fitted by an equivalent circuit, which is shown in the inset of Fig. 6(a) and the fitted parameters are listed in Table 1. R_e was derived from the contact resistance between the electrode and current collector and the interfacial resistance between the electrolyte and electrode, which corresponds to the high frequency intercept of the semicircle on the real axis. The semicircle at middle frequency was contributed by the charge-transfer resistance R_{ct} , which is related to the kinetic reaction at the air electrode surface [27]. The capacitance of the double-layer at the air electrode surface is represented by the constant phase element (CPE) Q_{dl} . The straight sloping line at low frequency could be described by the Warbury impedance W_o arising from the diffusion of oxygen in the electrolyte [28]. The expression for the constant phase element (CPE) Q_{dl} is

$$Q_{dl} = \frac{1}{Q_o(j\omega)^\alpha} \quad (1)$$

where ω is the angular frequency, j is the imaginary unit and the factor α is less than 1. When $\alpha=1$, a CPE represents a capacitor with capacitance of C [29,30].

The parameters used to fit the EIS from a Li–air cell before and after discharge are listed in Table 1. Both R_e and R_{ct} increased. The increase in R_e was due not only to the production of insulating discharge products after discharge, but also to the volume change of the Li–air cell before and after discharge [29]. The increase in R_{ct} mainly resulted from the blocking of the oxygen diffusion channel at the porous air electrode after discharge. As shown in Fig. 6(b) and Table 1, R_{ct} of the Li–air cell based on Fe_3O_4 /graphene composite was much smaller than that of the Li–air cell based on Fe_3O_4 NPs. The EIS results further showed that the Fe_3O_4 /graphene composite had an excellent catalytic activity.

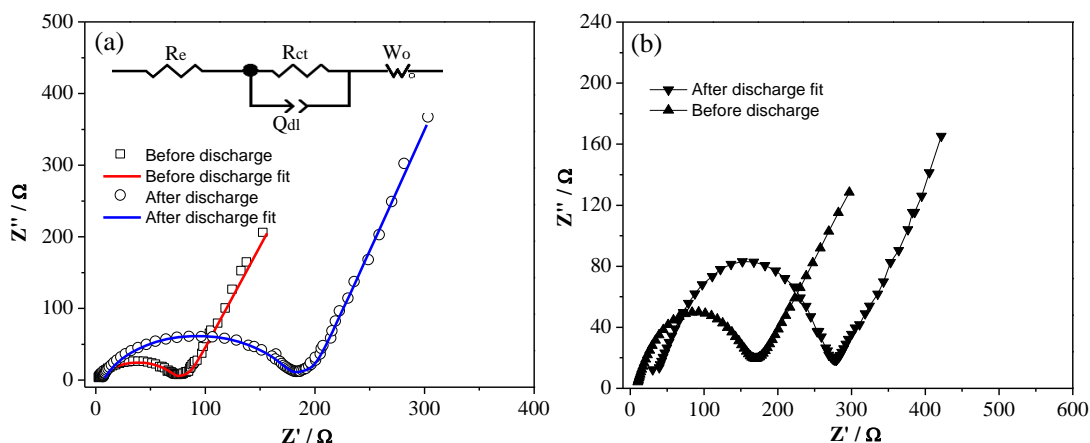


Figure 6. Impedance spectrum of Li–air cell based on different catalysts before and after discharge at 50 mA g⁻¹. The inset is the equivalent circuit used to fit EIS. (a) Fe_3O_4 /graphene nanocomposite; (b) Fe_3O_4 NPs

Table 1. Equivalent circuit parameters obtained from simulation of EIS experimental data.

Parameter	R_s / Ω	R_{ct} / Ω	CPE-T / F	CPE-P	W_o / Ω	W-T / F	W-P
Before discharge (Fe_3O_4 /GCs)	3.553	86.87	1.8497×10^{-5}	0.79491	43.28	2.152	0.41311
After discharge (Fe_3O_4 /GCs)	7.144	167.5	8.8152×10^{-6}	0.79632	67.24	1.969	0.40868

Before discharge (Fe_3O_4 NPs)	8.033	154.7	1.6252×10^{-5}	0.71014	343.2	7.64	0.58754
After discharge (Fe_3O_4 NPs)	35.47	236.6	4.5622×10^{-6}	0.74236	474.4	5.497	0.51852

To gain a better understanding of the discharge products in the air electrode of the Li–air cell with a Fe_3O_4 /graphene composite catalyst, FTIR analysis of the cathode both before and after discharge state were carried out. Fig. 7 shows the FTIR spectrum of the Fe_3O_4 /graphene composite cathode. The FTIR spectrum of the discharged electrode showed that the discharge products were undesirable Li_2CO_3 and expected Li_2O_2 . Accumulation of products which are not entirely oxidised on charge, Li parasitic reactions with air, the Li_2O_2 reacts chemically with H_2O and electrolyte starvation results in termination of cycling and capacity fading. The cyclic performance of lithium–air battery in ambient air is poor. We will put more effort to prolong the cyclic life of lithium–air batteries in ambient air.

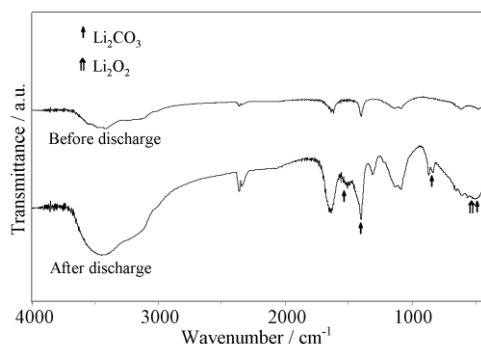


Figure 7. FTIR spectra of the air electrode before and after discharge.

4. CONCLUSIONS

A novel litchi-like Fe_3O_4 /graphene composite as cathode catalysts of lithium–air batteries was successfully prepared by a solvothermal method. In the Fe_3O_4 /graphene composite, litchi-like Fe_3O_4 which could provide a larger electrochemical reaction surface was homogeneously anchored on ultrathin flexible graphene sheets, which helped to maximize the effect of catalyst particles. The results of charge/discharge tests revealed that the Fe_3O_4 /graphene composite as cathode catalysts of lithium–air batteries exhibited a low charge potential, high discharge capacity, as well as high energy efficiency.

ACKNOWLEDGMENTS

The authors acknowledge financial supports from the Fundamental Research Funds for the Central Universities (2010LKHX05), the Specialized Research Fund for the Doctoral Program of Higher Education of China (20100095110009), and A Project Funded by the Priority Academic Program

Development of Jiangsu Higher Education Institutions. Thanks to Dr. Edward C. Mignot, Shandong University, for linguistic advice.

References

1. J. X. Zhu, D. Yang, Z. Y. Yin, Q. Y. Yan, H. Zhang, *Small*, 10 (2014) 3480
2. Y. Y. Shao, S. Park, J. Xiao, J. G. Zhang, Y. Wang, J. Liu, *ACS Catal.*, 2 (2012) 844
3. A. Debart, J. Bao, G. Armstrong, P. G. Bruce, *J. Power Sources*, 174 (2007) 1177
4. H. G. Jung, Y. S. Jeong, J. B. Park, Y. K. Sun, B. Scrosati, Y. J. Lee, *ACS Nano*, 7 (2013) 3532
5. D. Zhang, R. S. Li, T. Huang, A. S. Yu, *J. Power Sources*, 195 (2010) 1202
6. Y. M. Cui, Z. Y. Wen, Y. Liu, *Energy Environ Sci.*, 4 (2011) 4727
7. A. Debart, A. J. Paterson, J. Bao, P. G. Bruce, *Angew. Chem. Int. Ed.*, 47 (2008) 4521
8. C. Wang, H. Daimon, S. H. Sun, *Nano Lett.*, 9 (2009) 1493
9. A. Kraysberg, Y. E. Eli, *Nano Energy*, 2 (2013) 468
10. A. K. Thapa, T. Ishihara, *J. Power Sources*, 196 (2011) 7016
11. C. J. Fu, G. G. Zhao, H. J. Zhang, S. Li, *Int. J. Electrochem. Sci.*, 9 (2014) 46
12. D. Y. Chen, G. Ji, Y. Ma, J. Y. Lee, J. M. Lu, *ACS Appl. Mater. Interfaces*, 3 (2011) 3078
13. B. Wang, Y. Wang, J. Park, H. Ahn, G. X. Wang, *J. Alloys Compd.*, 509 (2011) 7778
14. Z. H. Yan, M. Wang, B. X. Huang, R. M. Liu, J. S. Zhao, *Int. J. Electrochem. Sci.*, 8 (2013) 149
15. Y. L. Dong, H. G. Zhang, Z. U. Rahman, L. Su, X. J. Chen, J. Hu, X. G. Chen, *Nanoscale*, 4 (2012) 3969
16. L. L. Tian, Q. C. Zhuang, J. Li, C. Wu, Y. L. Shi, S. G. Sun, *Electrochim. Acta*, 65 (2012) 153
17. E. L. Ma, J. J. Li, N. Q. Zhao, E. Z. Liu, C. N. He, C. S. Shi, *Mater. Lett.*, 91 (2013) 209
18. C. J. Zhou, W. J. Zhang, H. X. Wang, H. Y. Li, J. Zhou, S. H. Wang, J. Y. Liu, J. Luo, B. S. Zou, J. D. Zhou, *Arab. J. Sci. Eng.*, 39 (2014) 6679
19. L. Y. Jing, A. P. Fu, H. L. Li, J. Q. Liu, P. Z. Guo, Y. Q. Wang, X. S. Zhao, *RSC Adv.*, 4 (2014) 59981
20. W. S. Hummers, R. E. Offeman, *J. Am. Chem. Soc.*, 80 (1958) 1339
21. X. M. Sun, Z. Liu, K. Welsher, J. T. Robinson, A. Goodwin, S. Zaric, H. J. Dai, *Nano Res.*, 1 (2008) 203
22. C. M. Chen, Q. H. Yang, Y. G. Yang, W. Lv, Y. F. Wen, P. X. Hou, M. Z. Wang, H. M. Cheng, *Adv. Mater.*, 21 (2009) 3007
23. T. Nakajima, Y. Matsuo, *Carbon*, 32 (1994) 469
24. S. Park, J. An, J. R. Potts, A. Velamakanni, S. Murali, R. S. Ruoff, *Carbon*, 49 (2011) 3019
25. X. D. Huang, X. F. Zhou, K. Qian, D. Y. Zhao, Z. P. Liu, C. Z. Yu, *J. Alloys Compd.*, 514 (2012) 76
26. B. Sun, B. Wang, D. W. Su, L. D. Xiao, H. Ahn, G. X. Wang, *Carbon*, 50 (2012) 727
27. G. Q. Zhang, J. P. Zheng, R. Liang, C. Zhang, B. Wang, M. Au, M. Hendrickson, E. J. Plichta, *J. Electrochem. Soc.*, 158 (2011) A822
28. Y. Li, Y. Yin, K. Guo, X. Z. Xue, Z. Q. Zou, X. M. Li, T. He, H. Yang, *J. Power Sources*, 241 (2013) 288
29. G. Q. Zhang, J. P. Zheng, R. Liang, C. Zhang, B. Wang, M. Hendrickson, E. J. Plichta, *J. Electrochem. Soc.*, 157 (2010) A953
30. Q. C. Zhuang, T. Wei, L. L. Du, Y. L. Cui, L. Fang, S. G. Sun, *J. Phys. Chem. C*, 114 (2010) 8614